Anomalous Pseudocapacitive Behavior of a Nanostructured, Mixed-Valent Manganese Oxide Film for Electrical Energy Storage

Min-Kyu Song,[†,#] Shuang Cheng,[†,#] Haiyan Chen,[‡] Wentao Qin,[†] Kyung-Wan Nam,[§] Shucheng Xu,[||] Xiao-Qing Yang,[§] Angelo Bongiorno,[||] Jangsoo Lee,[⊥] Jianming Bai,[¶] Trevor A. Tyson,[‡] Jaephil Cho,[⊥] and Meilin Liu*,[†,#]

[†]School of Materials Science and Engineering, Center for Innovative Fuel Cell and Battery Technologies, Georgia Institute of Technology, 771 Ferst Drive, Atlanta, Georgia 30332-0245, United States

[‡]Department of Physics, New Jersey Institute of Technology, Newark, New Jersey 07102, United States

[§]Chemistry Department, Brookhaven National Laboratory, Upton, New York 11973, United States

[||]School of Chemistry and Biochemistry, Georgia Institute of Technology, 901 Atlantic Drive, Atlanta, Georgia 30332-0400, United States

[⊥]Interdisciplinary School of Green Energy, Ulsan National Institute of Science & Technology (UNIST), 701-11,100 Banyeon-ri, Eonyang-eup, Ulju-gun, Ulsan, Korea, 689-798

[¶]High Temperature Materials Laboratory, Oak Ridge National Laboratory, Oak Ridge, Tennessee 37831, United States

S *Supporting Information*
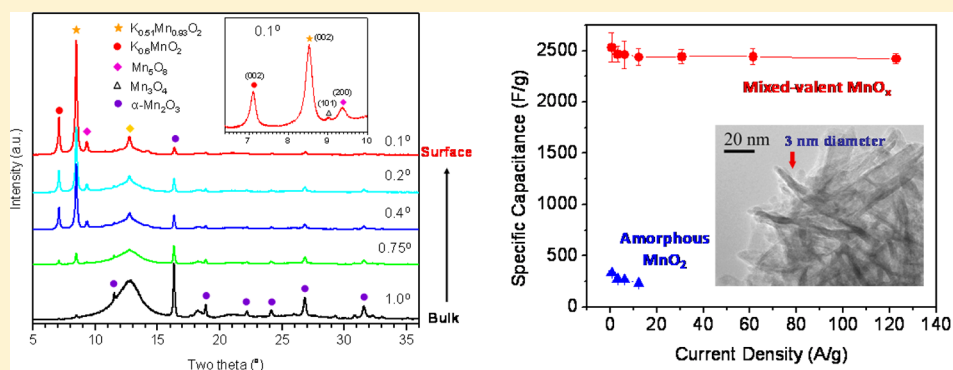
ABSTRACT: While pseudocapacitors represent a promising option for electrical energy storage, the performance of the existing ones must be dramatically enhanced to meet today's ever-increasing demands for many emerging applications. Here we report a nanostructured, mixed-valent manganese oxide film that exhibits anomalously high specific capacitance ($\sim$2530 F/g of manganese oxide, measured at 0.61 A/g in a two-electrode configuration with loading of active materials $\sim$0.16 mg/cm^2) while maintaining excellent power density and cycling life. The dramatic performance enhancement is attributed to its unique mixed-valence state with porous nanoarchitecture, which may facilitate rapid mass transport and enhance surface double-layer capacitance, while promoting facile redox reactions associated with charge storage by both Mn and O sites, as suggested by in situ X-ray absorption spectroscopy (XAS) and density functional theory calculations. The new charge storage mechanisms (in addition to redox reactions of cations) may offer critical insights to rational design of a new-generation energy storage devices.

KEYWORDS: Energy storage, electrochemical capacitors, mixed-valent compounds, enhanced pseudocapacitance, in situ X-ray absorption spectroscopy

While the application of existing batteries is often limited by low power, short cycle life, and long charging time,[1] the use of conventional capacitors suffers from inadequate energy density. Pseudocapacitors may bridge the gap between batteries and capacitors.[2] Unlike electrochemical double layer capacitors (EDLCs), which store electrical energy by accumulation of ions on electrode surface,[3] pseudocapacitors make use of fast redox reactions or phase changes on the surface or subsurface of electrodes,[4−6] offering much higher

energy densities than EDLCs. However, the rate capability and cycling stability of pseudocapacitors are perceived to be inferior to those of EDLCs and the energy density to be much lower than those of available batteries. To overcome these limitations, considerable efforts have been devoted to the creation of new
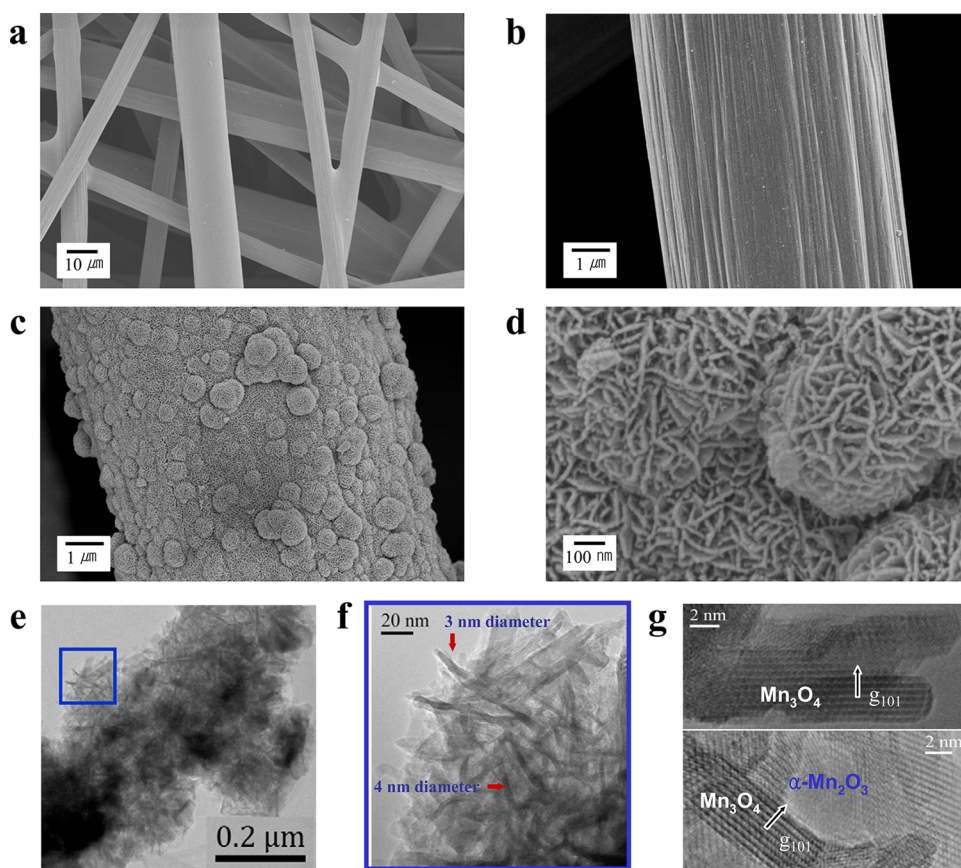
Figure 1. Electron microscopy analysis. (a) SEM image of carbon fiber paper (CFP) before coating showing 3D interconnected, porous structures. (b) SEM image of a carbon fiber before coating. (c) SEM image of a carbon fiber after conformal coating of MnO_x for 30 min. (d) SEM image of the MnO_x coating annealed at 400 °C in air for 2 h. (e) TEM image of MnO_x coating annealed at 400 °C in air for 2 h. (f) A zoomed-in view of the blue square area in (e) showing a cluster of the needle-shaped crystals with diameters of ~3 to ~4 nm. (g) High-resolution TEM images showing the fringes of Mn_3O_4 and α-Mn_2O_3 phase.

materials for pseudocapacitors. To date, however, the progress has been hindered largely by the lack of a profound understanding of the complex charge storage mechanisms related to intercalation of ions into electrode materials (of layered or channeled structures), reaction of ions with active electrode materials (to form new phases), and/or electrochemical adsorption of ions on electrode surfaces. It is traditionally believed that the pseudocapacitive behavior is associated primarily with the redox reactions of the cations (or changes in oxidation states of the cations) in electrode materials during operation.[2] A suitable electrode material for high performance should promote fast, reversible redox reactions on the surface or subsurface.[4,5]

Among many materials investigated, since first reported by Goodenough group,[7] MnO_2 has attracted much attention because it is abundant, inexpensive, and environmentally benign. While MnO_2 has high theoretical capacitance[8] (~1370 F/g as the oxidation state of Mn ion is changed from 4+ to 3+ over a potential window of 0.8 V), its poor electronic conductivity often limits the electrode utilization; only the surface layers may participate in redox reactions. To overcome this limitation, MnO_2 has been mixed with carbon particles or loaded onto carbon supports (including carbon nanotubes and graphene).[9−16] To date, however, the reported specific capacitance of MnO_2 varies from ~150 to ~940 F/g while the cycling stability still needs further improvement. Although higher specific capacitance (~1145 F/g) has been

reported,[17] the MnO_2 was deposited into a nanoporous gold film (~100 nm thick) and thus could be less competitive economically for practical applications. Further, the rate capability is still unsatisfactory for large-scale applications such as auxiliary power units for electric vehicles. With several oxidation states and a wide range of phases, manganese is a vital component in photosynthetic systems due to its unique ability to cycle between various oxidation states.[18] In particular, manganese oxides can assume many different crystal structures upon accommodation of other metal cations. These complex features often give rise to unusual properties of manganese oxide. For example, the dramatic enhancement of catalytic activities toward oxidation of various organic compounds was attributed to the mixed-valence of manganese oxides.[19,20]

The investigation of mixed-valent compounds has a long and interesting history. Mixed-valent compounds contain donor and acceptor sites separated by a bridge. Since Prussian blue, a complex Fe(II)/Fe(III) cyanide, was first discovered in 1704, the study of mixed-valent compounds has had significant impacts in chemistry, physics, and biology. In particular, from the late 1960s, molecular mixed-valent compounds began to receive great attention due to their unique optical properties arising from significant electron transitions between donor and acceptor sites by absorbing specific wavelengths of visible light via intervalence charge transfer. The intense blue color of Prussian blue is related to the energy of the electron transfer from Fe(II) to Fe(III). Two key factors (and their interaction)

that determine their unique properties are the "electronic coupling" between the two redox sites, and the "reorganization energy" associated with electron transfer between them.[21] Charge localization or delocalization has been a central issue in mixed-valence chemistry. By a classification scheme proposed by Robin and Day,[22] mixed-valent compounds can be completely localized, fully delocalized, or systems in between, depending on the strength of the electron interaction between the oxidized and reduced sites. To date, compounds of group 8−11 transition metals have been most intensively studied. In particular, compounds of iron, ruthenium, platinum, and copper have been widely studied.[23] For example, many mixed-valent copper-based oxides have been developed as superconductors. The compound $YBa_2Cu_3O_7$ has mixed-valent Cu(II) and Cu(III). Also, a number of rare-earth compounds with atomic-like f levels coexisting with wide s−d band at the Fermi level have shown very unique thermal and magnetic properties.[24]

However, the nature of the mixed-valent chemistry on the surface of nanostructured materials has not yet been fully understood and a fundamental understanding of the relationship between mixed-valent structure and properties is still lacking. It should be also noted that the mixed-valence chemistry of the early transition metals is considerably less well established, yet a remarkable variety of structurally diverse mixed-valence compounds can be formed from these elements. Their wide range of oxidation states, coordination numbers, and geometries can offer great potential for the formation of unique mixed-valent compounds, and many of these may exhibit distinctive bonding, chemistry, and properties suitable for various applications. In particular, although early transition elements such as titanium, vanadium, and manganese are important in biology, catalysis, artificial photosynthesis, and energy storage/conversion science, the controlled synthesis of their mixed-valent compounds and their unique electrochemical properties have not yet been explored. In this paper, we demonstrated the controlled synthesis of nanostructured, mixed-valent manganese oxides and explored their unique properties as electrodes for high-performance pseudocapacitors.

We used conductive and porous carbon fiber paper (CFP) as both the current collector and the electrode for conformal coating of mixed-valence MnO_x as the active electrode material for pseudocapacitors (Figure 1a,b). Individual carbon fibers in the CFP are well-connected and the pores are sufficiently large to allow efficient ion access to all surface area of the electrode. We deposited a thin, uniform coating of nanoporous MnO_x directly onto porous CFP using a simple precipitation method in an aqueous solution at 75 °C (Figure 1c,d). The porous network structure of the CFP is retained because the conformal MnO_x coating is relatively thin, as revealed by microscopy. The MnO_x coated CFP were then heat-treated at 200−450 °C in different atmospheres (air, N_2, and 4% H_2). TEM analysis of the samples annealed at 400 °C in air for 2 h revealed that the MnO_x films consist of many low aspect-ratio crystals (each being a few tens of nanometers in size) as well as clustered and needle-shaped crystals, whose diameters vary from a few nanometers to ~10 nm (Figure 1e−g, Supporting Information S1). Selected area electron diffraction (SAED) analysis (Supporting Information Figure S1b) suggested that the low-aspect ratio nanocrystals examined are α-Mn_2O_3 with a lattice constant of 0.94 nm, and the needle-shaped crystals were identified as Mn_3O_4 (Hausmannite) based on lattice images (Figure 1g). The lattice fringes reveal the axes of the two

needle-shaped Mn_3O_4 crystals are parallel to the (101) lattice planes (Supporting Information Figure S1c). Since both the (101) and (011) spacing are the largest lattice spacing in the Mn_3O_4 lattice, such an orientation may facilitate the incorporation and transport of ions along this direction. The thickness of MnO_x coating varied from ~70 to ~800 nm (Supporting Information Figure S2−S4), depending on the deposition time (2 to 30 min).

To further characterize the structural features of the MnO_x coatings formed on CFP, we used both laboratory and synchrotron-based X-ray diffraction (XRD) analysis. Figure 2a
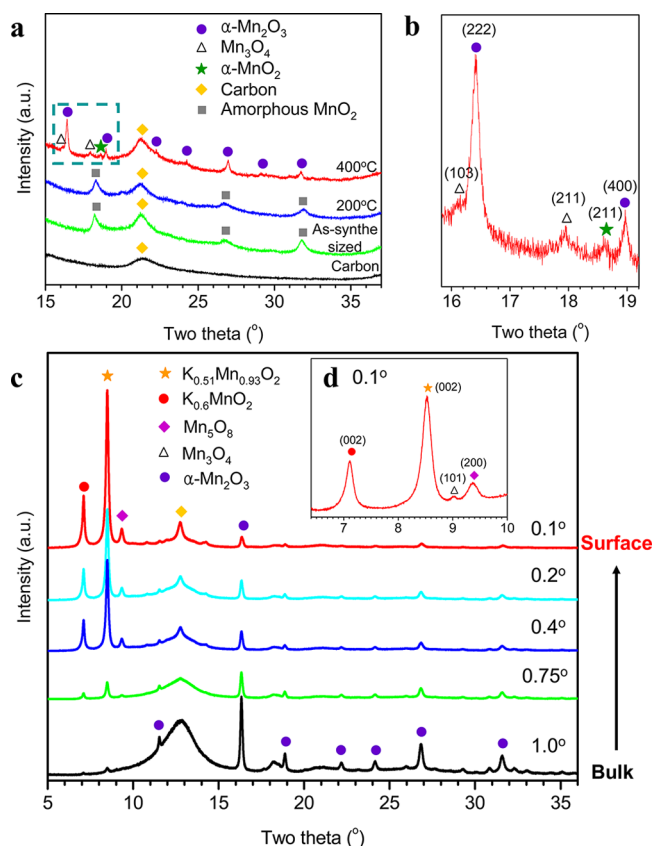
Figure 2. Synchrotron XRD analysis. (a) Transmission mode XRD pattern: bare carbon paper before coating, MnO_x electrodes before and after annealing at different temperatures (200 and 400 °C) in air for 2 h. (b) Enlarged view of XRD pattern between 16−19° of XRD pattern of MnO_x annealed at 400 °C in air for 2 h and highlighted in Figure 2a. (c) XRD pattern at of MnO_x annealed at 400 °C in air for 2 h measured at different incident angle (0.1−1°). (d) XRD pattern at incident glancing angle of 0.1° of MnO_x annealed at 400 °C in air for 2 h showing the representative surface species.

shows the synchrotron-based XRD patterns (transmission mode) of samples (deposited for 30 min) before and after annealing in air at different temperatures. The very broad characteristic peaks in the XRD patterns indicated that the as-deposited MnO_2 coating was amorphous and remained so after annealing at 200 °C in air for 2 h, which is consistent with previous studies under similar synthesis conditions.[25,26] The amorphous phase of MnO_2 was believed to be good electrode materials for pseudocapacitors.[7,26,27] When annealed with CFP at 400 °C in air for 2 h, the amorphous MnO_2 was converted to crystalline α-Mn_2O_3 with small amount of Mn_3O_4 (Hausmannite) and α-MnO_2, as evident from the XRD patterns shown in
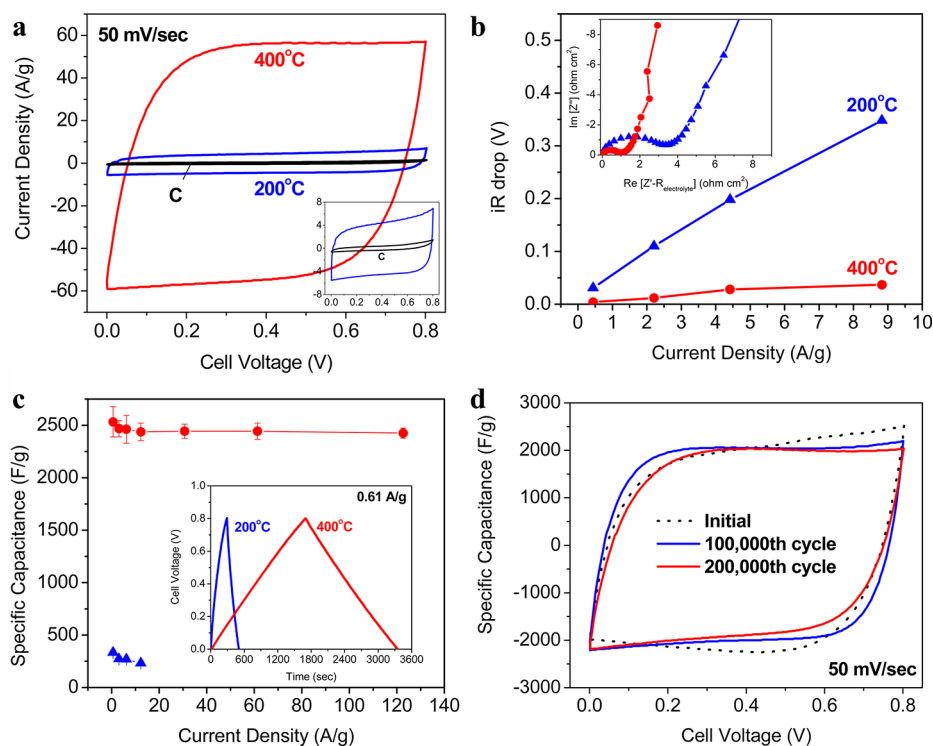
Figure 3. Electrochemical performance of symmetric pseudocapacitors constructed from amorphous MnO_2 and mixed-valent MnO_x electrodes. (a) Cyclic voltammograms measured between 0−0.8 V at a scan rate of 50 mV/s. (b) iR drop of the cells measured at different current densities. Insert shows electrochemical impedance spectra collected at open circuit voltage under the influence of an ac voltage of 10 mV. (c) Specific capacitance at different current densities demonstrating superior rate-capability. Insert shows typical charge−discharge curves of amorphous MnO_2 and mixed-valent MnO_x electrodes at a constant current density of 0.61A/g. Only the weight of the active electrode material (MnO_x, ∼0.32 mg) was considered in the specific capacitance calculations. (d) Cyclic voltammograms before and after long-term cycling at a scan rate of 50 mV/s showing excellent cycling stability.

Figure 2a,b. These crystalline phases started to appear at ∼360 °C when the temperature was raised from 200 to 400 °C in air, as revealed by the in situ XRD analysis (Supporting Information Figure S5). It is noted, however, that the transmission-mode XRD pattern is quite different from those collected at a small glancing angle (Supporting Information Figure S6), suggesting that the phases on the surface are very different from those in the bulk.

To gain some insights into the structures of the surface layer, we collected XRD patterns at different glancing incident angles (Figure 2c,d). A lower incident angle corresponds to a shallower penetration depth of the X-ray, allowing us to probe the structure of a layer closer to the surface. When the incident angle was varied from 1 to 0.1°, the α-Mn_2O_3 peaks decreased gradually while the peaks corresponding to K-incorporated MnO_2 ($K_{0.6}MnO_2$ and $K_{0.51}Mn_{0.93}O_2$) and Mn_5O_8 increased considerably, suggesting that α-Mn_2O_3 is present predominantly in the bulk whereas the K-incorporated MnO_2 and Mn_5O_8 are formed mostly near the surface (Figure 2d). It is noted that small peaks corresponding to Mn_3O_4 were observable in both transmission-mode and glancing angle mode XRD patterns, implying that small amount of Mn_3O_4 is present in the bulk and on the surface. This is consistent with TEM observation (Figure 1g). The surface phases (K-incorporated MnO_2, Mn_5O_8, and Mn_3O_4) were formed at 400 °C, as indicated by the low glancing angle XRD analysis at different temperatures (Supporting Information Figure S7).

XRD analysis of the mixed-valent MnO_x of different thicknesses suggests that the predominating phase of the ∼800 nm films (deposited for 30 min) was α-Mn_2O_3 whereas

that of the ∼70 nm films (deposited for 2 min) was Mn_3O_4, which showed the highest specific capacitance. As the thickness was reduced (Supporting Information Figure S8), the predominating "bulk" phase was changed from α-Mn_2O_3 to a phase similar to Mn_3O_4. This is anticipated because the degree of MnO_x reduction (by the carbon substrate) decreases in the direction away from the carbon substrate surface, which was exposed to air. The annealing condition created a gradient in oxidation state of Mn ion along the thickness direction; thinner MnO_x films deposited on carbon fiber were more reduced. However, they were still mixed-valent MnO_x and there is more Mn_3O_4 phase in a thinner film (Supporting Information Figure S8−S10). It is noted that all electrodes deposited for 2, 5, 15, and 30 min have the same surface phases; the graded oxidation state remained largely the same.

Gas adsorption/desorption analysis implied that the microstructure of MnO_x underwent a dramatic rearrangement during the annealing process, producing porous, nanostructured MnO_x (Supporting Information Figure S11). The specific surface area increased from 5.21 m^2/g for amorphous MnO_2 to 261.8 m^2/g for the multivalent MnO_x, as the pore volume increased from 0.021 to 0.149 cm^3/g (∼42% porosity) at the same time. The formation of tunneled structure of K-incorporated MnO_2 on the surface may partially account for enlarged surface area and pore volume.[18,28] The porous, nanostructured multivalent MnO_x is ideally suited for fast mass and charge transfer associated with energy storage processes.

To evaluate the characteristic behavior of the mixed-valent MnO_x electrodes for electrical energy storage, we performed several electrochemical measurements in a 1 M Na_2SO_4

solution. The mixed-valent MnO_x electrode showed excellent "square-shape" cyclic voltammograms at 50 mV/s (Figure 3a) with current densities being almost 1 order of magnitude higher than those of the amorphous MnO_2 electrode. The symmetric shape and the instant response upon the reversal of voltage indicate that surface reactions are highly reversible and very fast. It is noted that the contribution of the porous carbon fiber substrate to the capacitance is negligible.

We have also measured the internal resistance of the electrochemical capacitors when the potentials were reversed (Supporting Information Figure S12) and plotted them as a function of applied current densities (Figure 3b). The slopes of the plots correspond directly to the equivalent series resistances (ESR) of the capacitors. This internal resistance critically influences the power density (or rate capability) of electrochemical capacitors; low capacitance and deviation from ideal capacitor behavior are usually associated with large ESR. It is clearly shown that the mixed-valent MnO_x displayed much smaller ESR than the amorphous MnO_2 at a given current density due most likely to enhanced rates of the surface redox reactions. This observation was further confirmed by the impedance measurements (insert of Figure 3b). The charge-transfer resistance (the diameter of the semicircle in the impedance spectrum) of the mixed-valent MnO_x was much smaller than that of the amorphous MnO_2. The long tail at low frequencies of the mixed-valent MnO_x is closer to a vertical line for an ideal capacitor, another indication that the mixed-valent MnO_x has higher capacitance and lower resistance than the amorphous MnO_2.

Typical charge–discharge curves at a constant current of 0.61 A/g are shown in Figure 3c. The "linear" and symmetrical charge–discharge curves indicate again high Coulombic efficiency or excellent reversibility. The specific capacitance (calculated from the discharge curve) of the amorphous MnO_2 was 333 F/g, comparable to the values reported in the literatures.[26,29] In contrast, the specific capacitance for the mixed-valent MnO_x (of ~70 nm thick) was ~2530 F/g, almost eight times higher than that of the amorphous MnO_2 (of the same loading). This represents the highest specific capacitance ever reported among all known pseudocapacitor materials, including MnO_2 (1145 F/g; film <40 nm thick in a 100 nm porous Au film),[17] $Ni(OH)_2$ (1335 F/g; nanoplates <10 nm thick),[30] and RuO_2 (1340 F/g; nanodots with 2–3 nm in diameter)[31] when all normalized to the weight of the active material only.

Because high rate capability is the most important feature of electrochemical capacitors, we measured the performance at very high cycling rates. Typically, the capacitance of a pseudocapacitor may decrease with operating current density due to mass transport limitations, especially when insertion (or removal) of ions into (or from) the electrode subsurface is involved. Much to our surprise, however, the capacitance of the mixed-valent MnO_x was not kinetically limited even at very high cycling rates (Supporting Information Figure S13), demonstrating ~2430 F/g at 122.7 A/g. Further, the mixed-valent MnO_x electrode displayed remarkable long-term cycling stability; cyclic voltammograms collected after 100 000 and 200 000 cycles (Figure 3d) showed little change, whereas the capacitance of the amorphous MnO_2 was much lower and degraded considerably during cycling (Supporting Information Figure S14–15). It was also found that symmetric pseudocapacitors constructed from the mixed-valent MnO_x showed very

stable performance up to 1.0 V (Supporting Information Figure S16).

It is noted, however, that the specific capacitance drops with the thickness of the MnO_x film (or loading), suggesting that only a thin film was fully utilized (or the nanoporous surface phases make dominating contributions to the observed capacitance) (Supporting Information Figure S17–18). This is not surprising because the charge storage in a capacitor is primarily confined to the surface and subsurface (or a thin layer). To increase the performance of electrochemical capacitors by increasing the film thickness of active materials is proven ineffective and, perhaps, fundamentally unattainable; after all, the rate capability may ultimately diminish with film thickness. However, our results demonstrate that it may be unnecessary to increase film thickness because the charge storage capacity of the MnO_x film can be dramatically enhanced (~8 times) by creating mixed-valent nanostructure, achieving values much higher than the "theoretical capacity" previously believed (e.g., ~1370 F/g for MnO_2 under similar conditions).[8] Indeed, the estimated specific energy density of the ~70 nm thick mixed-valent MnO_x film (single electrode in a voltage window between 0 and 1.0 V) reached ~352 Wh/kg at a power density of ~614 W/kg and showed little dependence on cycling rate, still retaining ~337 Wh/kg at power densities up to ~117 800 W/kg (full charge or discharge in 10 s) when all normalized to the weight of active material only. The demonstrated specific energy densities of single electrode are much higher than those of the state-of-art pseudocapacitor materials[17,30] (Note the voltage window for MnO_2 and $Ni(OH)_2$ were 0.8 and 0.55 V in two- and three-electrode configuration, respectively) and even comparable to those of high-performance battery materials such as $FePO_4$ nanowires (~300 Wh/kg at ~4000 W/kg) and $Li(Ni_{0.5}Mn_{0.5})O_2$ (~600 Wh/kg at ~6000 W/kg) while retaining much higher gravimetric power (when all normalized to the weight of the electrode material only).[32,33] Although significantly improved performance has been achieved in this study with a nanoscale coating, the mixed-valent MnO_x shows great potential to provide an order of magnitude increase in practical energy density of electrochemical capacitors without penalizing power density. We believe that MnO_x coatings must be thin to offer the best possible power density. Therefore, one effective approach to increasing practical energy density (e.g., loading) without compromising the specific capacitance or rate capability is to use nanocarbon fibers, thus increasing the surface area of CFP for conformal coating of MnO_x.

The phase composition and nanostructure of the electrode material is very sensitive to the annealing conditions. For example, when the annealing temperature was increased from 400 to 450 °C (but still in air for 2 h), XRD analysis suggested that the Mn_3O_4 phase was converted to α-Mn_2O_3 (Supporting Information Figure S19). Similarly, when the annealing atmosphere was changed from air to N_2 and 4% H_2 balanced with Ar (still at 400 °C for 2 h), the as-synthesized amorphous MnO_2 on CFP was converted to pure Mn_3O_4 and a mixture of MnO and Mn_3O_4, respectively (Supporting Information Figure S20). Further, the amorphous MnO_2 powder sample (synthesized under the same conditions but without carbon support) remained amorphous when annealed at 400 °C, but transformed to crystalline α-Mn_2O_3 when annealed at 500 °C, in air for 2 h in the absence of carbon (Supporting Information Figure S21). Electrodes made of these phases performed poorly, far inferior to that of the electrodes made of the
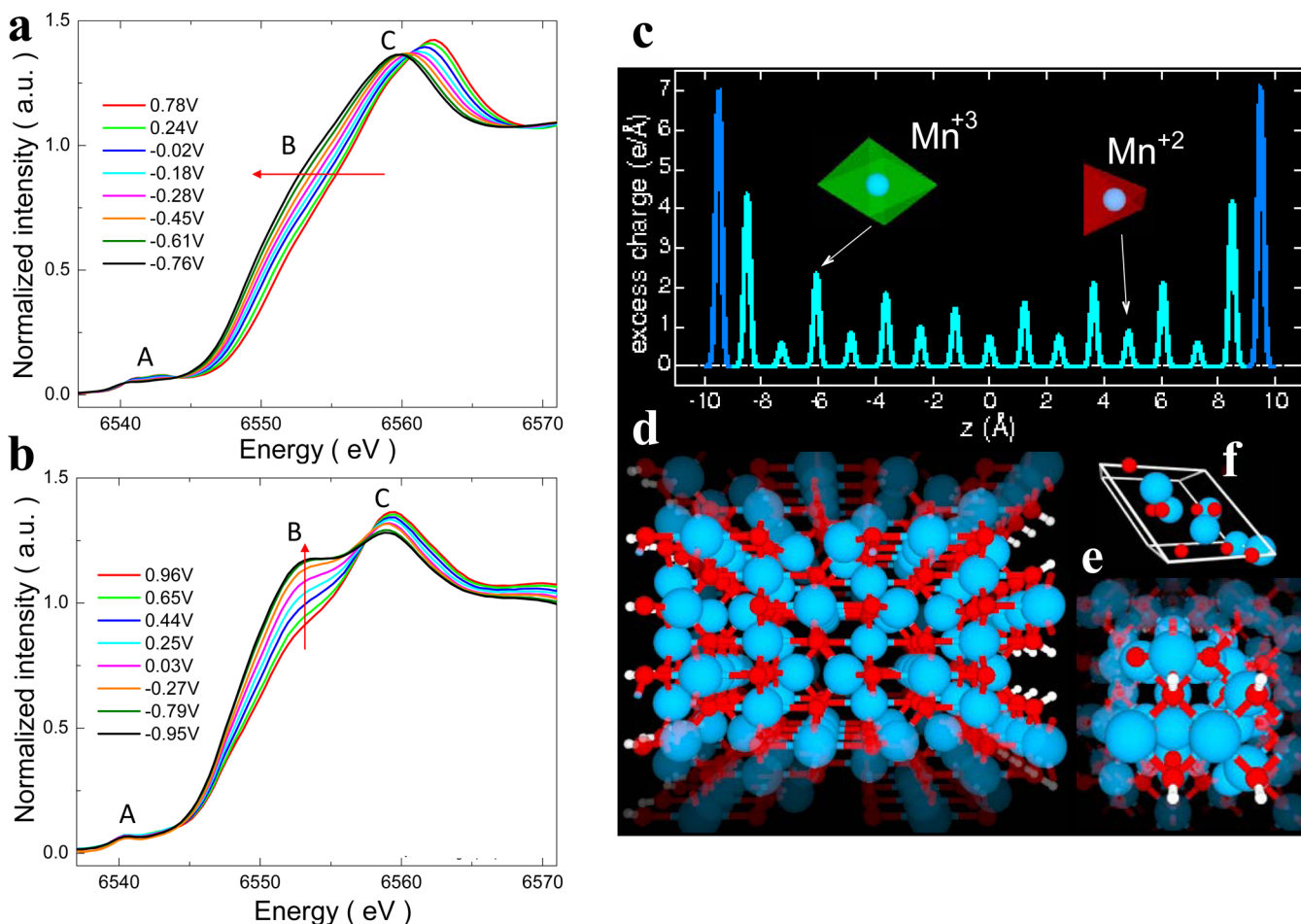
Figure 4. Investigation into the charge storage mechanism. (a) In situ XANES spectra of the as-synthesized (amorphous MnO_2) and (b) the mixed-valent MnO_x electrode during discharge in 1.0 M Na_2SO_4 electrolyte. A, B, and C represent pre-edge (1s → 3d transition), covalent character between Mn(3d) and O(2p) bond due to LMCT, and main edges (1s → 4p transition). (c) Linear excess charge distribution across the slab of Mn_3O_4 as derived from PBE+U calculations. The distribution is normalized to the number of excess electrons added to the slab model. The charge accumulated at the surface is shown in blue, while the cyan color is used to show the charge distribution in the bulk stored in the $[MnO_4]$ tetrahedra and $[MnO_6]$ octahedra, respectively. (d) Side view and (e) top view of the slab used in the PBE+U calculations. (f) Primitive unit cell of Mn_3O_4. Mn and O atoms are shown in blue and red colors, respectively.

multivalent MnO_x created by annealing in air at 400 °C for 2 h (Supporting Information Figure S19−S20).

Since the mixed-valent phases seem to play a pivotal role in achieving the anomalously high capacitance, we performed both ex situ and in situ XAS to gain some insights into the charge-storage mechanism of the mixed-valent MnO_x electrodes (Supporting Information Figure S22−S23). The in situ X-ray absorption near edge spectroscopy (XANES) spectra (Figure 4a) for the as-synthesized MnO_2 electrodes acquired during the first discharge (0.8 to −0.8 V) showed an entire edge shift toward lower energy in a continuous manner, suggesting that the charge storage is mostly associated with the Mn^{3+}/Mn^{4+} redox reactions, as conventionally believed. In contrast, however, the XANES spectra (Figure 4b) for the mixed-valent MnO_x collected under the identical conditions (except over a wider voltage window from 1.0 to −1.0 V) showed completely different spectral features that have never before been reported. First, there was no obvious entire edge shift during discharge, although a slight edge shift toward lower energy was observed, indicating a decrease in average oxidation state of Mn ions. The average change in Mn valence (calculated from the edge shift) for both cases was similar: ∼0.3 within a voltage window of 0.0

to 0.8 V (Supporting Information Figure S23); yet, the observed specific capacitance for the mixed-valent MnO_x is much higher (∼8 times) than that for the as-prepared MnO_2 sample. Clearly, the change in oxidation state of Mn ion cannot account for the anomalous pseudocapacitive behavior. Second, the dominating spectral feature is a unique evolution of the shoulder peak (B), which is related to the ligand-to-metal charge transfer (LMCT) process. The increased B peak intensity indicates the increased degree of covalent character of Mn(3d)-O(2p) bonding during the discharge. Thus, the unique Mn K-edge change in the form of increasing B feature clearly shows that a large portion of the charge compensation might be originated from the hole state redistribution toward the oxygen sites, rather than just the reduction of Mn ion (as seen for the as-synthesized MnO_2), suggesting that the unique atomic and electronic structure (Supporting Information Figure S22) of the nanostructured, mixed-valent MnO_x may allow additional charge compensation mechanism, which has not been observed in MnO_2. Although small intensity change of B feature in XANES spectra during charge−discharge were reported in the literature[34,35] for transition metal K-edges such as Co and Mn, it has never before been observed that

these spectral changes (LMCT) play a dominating role over the continuous edge shift (redox reaction of cations).

The role of oxygen anions for charge compensation in transition metal oxides is not unprecedented; it was previously argued for lithium battery electrodes. Aydinol et al. showed that more charge can be transferred to the oxygen anions than to the metal cations in the oxide upon intercalation of lithium ions.[36] To estimate the charge distribution in the nanoporous multivalent MnO_x (with dominant phase of Mn_3O_4), we resorted to spin-polarized density functional theory (DFT) calculations. To model the geometry of Mn_3O_4 nanoneedles (as seen in Figure 1g), we used a tetragonal slab of Mn_3O_4 exposing to the vacuum two opposite (001) surfaces of area 5.94×5.94 Å^2 and having a linear dimension perpendicular to the surface of 19.5 Å. Our DFT calculations (Figure 4c) show that significant amount of the excess negative charge is indeed accumulated at the surface of the Mn_3O_4 nanoneedles. In the bulk, the excess negative charge gradually decays from the surface peak, localizing prevalently in correspondence of the Mn^{3+} ions in the $[MnO_6]$ octahedra rather than at the Mn^{2+} centers in the $[MnO_4]$ tetrahedra. An analysis of the individual Bader atomic charges[37] shows, in particular, that the percentage of excess charge stored at the surface and in the bulk of Mn_3O_4 is 36 and 64%, respectively, while in the bulk the negative charge accumulated at or in proximity of Mn^{2+}, Mn^{3+}, and O centers is 15, 50, and 35%, respectively.

Our DFT calculations therefore suggest that the amounts of excess charge accumulated on the surface and at O centers are significant, consistent with our in situ XAS results. Charge accumulation on O centers appear to be favored by the close proximity of the Mn^{3+} species that, thanks to the good hybridization of the Mn^{3+} 3d and the O 2p orbitals, spill the excess negative charge onto the neighboring O atoms. These new charge compensation mechanisms at O centers and surfaces directly challenge the traditional notion that pseudocapacitance is primarily associated with redox reaction of cations.

Additionally, the coexistence of aliovalent cations (Mn^{2+}, Mn^{3+}, and Mn^{4+}) may facilitate the formation of more ionic defects (e.g., vacancies and misplaced ions) and electronic defects (electrons and holes), thus altering the electronic, ionic, and catalytic properties of the manganese oxides. These defects may accelerate the kinetics of the surface redox reactions. Also, the mismatches induced by structural differences among different manganese oxide phases may produce additional defects (cavities, stacking faults, etc.), thus facilitating the formation of porous nanoarchitectures that may enhance the transport of charged species and extend the reaction sites from the surface to the subsurface of electrode. Recent theoretical studies predicted that photoconductivity of MnO_2 can be enhanced by introducing Ruetschi defects or protonated Mn(IV) vacancies, suggesting that electronic properties can be tailored by tuning the defect structure during synthesis.[38]

Our results suggest that electrochemical capacitors based on this MnO_x film have potential to reach energy densities much higher than those of existing pseudocapacitors while maintaining high rate capabilities and excellent cycling performance of EDLCs. This can be accomplished by the creation of thin films of mixed-valent manganese oxides with porous nanoarchitecture, enabling multiple charge storage mechanisms with much smaller internal resistance and highly reversible, faster charge transfer kinetics. Although we have focused on MnO_x as active materials for pseudocapacitors in this study, other transition metal oxides could also be explored using a similar method to design mixed-valent nanostructures/carbon composites with significantly enhanced electrochemical performances for other applications.

■ ASSOCIATED CONTENT

Ⓢ Supporting Information

Additional figures and experimental details are included. This material is available free of charge via the Internet at http://pubs.acs.org.

■ AUTHOR INFORMATION

Corresponding Author

*E-mail: meilin.liu@mse.gatech.edu.

Author Contributions

#These authors contributed equally to this work.

Notes

The authors declare no competing financial interest.

■ ACKNOWLEDGMENTS

■ REFERENCES

(1) Whittingham, M. S. *MRS Bull.* **2008**, *33* (4), 411−419.

(2) Conway, B. E. *Electrochemical Supercapacitors*; Kluwer-Academic: New York, 1999.

(3) Chmiola, J.; Yushin, G.; Gogotsi, Y.; Portet, C.; Simon, P.; Taberna, P. L. *Science* **2006**, *313* (5794), 1760−1763.

(4) Simon, P.; Gogotsi, Y. *Nat. Mater.* **2008**, *7* (11), 845−854.

(5) Hall, P. J.; Mirzaeian, M.; Fletcher, S. I.; Sillars, F. B.; Rennie, A. J. R.; Shitta-Bey, G. O.; Wilson, G.; Cruden, A.; Carter, R. *Energy Environ. Sci.* **2010**, *3* (9), 1238−1251.

(6) Brezesinski, T.; Wang, J.; Tolbert, S. H.; Dunn, B. *Nat. Mater.* **2010**, *9* (2), 146−151.

(7) Lee, H. Y.; Goodenough, J. B. *J. Solid State Chem.* **1999**, *144* (1), 220−223.

(8) Toupin, M.; Brousse, T.; Belanger, D. *Chem. Mater.* **2004**, *16* (16), 3184−3190.

(9) Yu, G.; Hu, L.; Liu, N.; Wang, H.; Vosgueritchian, M.; Yang, Y.; Cui, Y.; Bao, Z. *Nano Lett.* **2011**, *11* (10), 4438−4442.

(10) Yu, G.; Hu, L.; Vosgueritchian, M.; Wang, H.; Xie, X.; McDonough, J. R.; Cui, X.; Cui, Y.; Bao, Z. *Nano Lett.* **2011**, *11* (7), 2905−2911.

(11) Hu, L.; Pasta, M.; Mantia, F. L.; Cui, L.; Jeong, S.; Deshazer, H. D.; Choi, J. W.; Han, S. M.; Cui, Y. *Nano Lett.* **2010**, *10* (2), 708−714.

(12) Raymundo-Pinero, E.; Khomenko, V.; Frackowiak, E.; Beguin, F. *J. Electrochem. Soc.* **2005**, *152* (1), A229−A235.

(13) Chou, S. L.; Wang, J. Z.; Chew, S. Y.; Liu, H. K.; Dou, S. X. *Electrochem. Commun.* **2008**, *10* (11), 1724−1727.

(14) Fischer, A. E.; Pettigrew, K. A.; Rolison, D. R.; Stroud, R. M.; Long, J. W. *Nano Lett.* **2007**, *7* (2), 281−286.

(15) Lee, S. W.; Kim, J.; Chen, S.; Hammond, P. T.; Shao-Horn, Y. *ACS Nano* **2010**, *4* (7), 3889−3896.

(16) Chen, S.; Zhu, J.; Wu, X.; Han, Q.; Wang, X. *ACS Nano* **2010**, *4* (5), 2822−2830.

(17) Lang, X. Y.; Hirata, A.; Fujita, T.; Chen, M. W. *Nat. Nanotechnol.* **2011**, *6* (4), 232−236.

(18) Post, J. E. *Proc. Natl. Acad. Sci. U.S.A.* **1999**, *96* (7), 3447−3454.

(19) Shen, Y. F.; Zerger, R. P.; Deguzman, R. N.; Suib, S. L.; McCurdy, L.; Potter, D. I.; Oyoung, C. L. *Science* **1993**, *260* (5107), 511−515.

(20) Tian, Z. R.; Tong, W.; Wang, J. Y.; Duan, N. G.; Krishnan, V. V.; Suib, S. L. *Science* **1997**, *276* (5314), 926−930.

(21) Hankache, J.; Wenger, O. S. *Chem. Rev.* **2011**, *111* (8), 5138−5178.

(22) Robin, M. B.; Day, P. Mixed Valence Chemistry-A Survey and Classification. In *Advances in Inorganic Chemistry*; Eméléus, H. J.; Sharpe, A. G., Eds.; Academic Press: New York, 1968; Vol. *10*, pp 247−422.

(23) Young, C. G. *Coord. Chem. Rev.* **1989**, *96*, 89−251.

(24) Varma, C. M. *Rev. Mod. Phys.* **1976**, *48* (2), 219−238.

(25) Ragupathy, P.; Park, D. H.; Campet, G.; Vasan, H. N.; Hwang, S. J.; Choy, J. H.; Munichandraiah, N. *J. Phys. Chem. C* **2009**, *113* (15), 6303−6309.

(26) Xu, M. W.; Zhao, D. D.; Bao, S. J.; Li, H. L. *J. Solid State Electrochem.* **2007**, *11* (8), 1101−1107.

(27) Subramanian, V.; Zhu, H. W.; Wei, B. Q. *Electrochem. Commun.* **2006**, *8* (5), 827−832.

(28) Gao, T.; Glerup, M.; Krumeich, F.; Nesper, R.; Fjellvag, H.; Norby, P. *J. Phys. Chem. C* **2008**, *112* (34), 13134−13140.

(29) Hu, C. C.; Tsou, T. W. *Electrochem. Commun.* **2002**, *4* (2), 105−109.

(30) Wang, H.; Casalongue, H. S.; Liang, Y.; Dai, H. *J. Am. Chem. Soc.* **2010**, *132* (21), 7472−7477.

(31) Hu, C. C.; Chen, W. C.; Chang, K. H. *J. Electrochem. Soc.* **2004**, *151* (2), A281−A290.

(32) Lee, Y. J.; Yi, H.; Kim, W. J.; Kang, K.; Yun, D. S.; Strano, M. S.; Ceder, G.; Belcher, A. M. *Science* **2009**, *324* (5930), 1051−1055.

(33) Kang, K. S.; Meng, Y. S.; Breger, J.; Grey, C. P.; Ceder, G. *Science* **2006**, *311* (5763), 977−980.

(34) Yoon, W. S.; Balasubramanian, M.; Chung, K. Y.; Yang, X. Q.; McBreen, J.; Grey, C. P.; Fischer, D. A. *J. Am. Chem. Soc.* **2005**, *127* (49), 17479−17487.

(35) Kim, M. G.; Shin, H. J.; Kim, J. H.; Park, S. H.; Sun, Y. K. *J. Electrochem. Soc.* **2005**, *152* (7), A1320−A1328.

(36) Aydinol, M. K.; Kohan, A. F.; Ceder, G.; Cho, K.; Joannopoulos, J. *Phys. Rev. B* **1997**, *56* (3), 1354−1365.

(37) Bader, R. F. W. *Atoms in Molecules - A Quantum Theory*; Oxford University Press: New York, 1990.

(38) Kwon, K. D.; Refson, K.; Sposito, G. *Phys. Rev. Lett.* **2008**, *100*, 146601.